9-1-2011

Quantification of renal perfusion: Comparison of arterial spin labeling and dynamic contrast-enhanced MRI

Jeff D. Winter
Hospital for Sick Children University of Toronto

Keith S. St. Lawrence
Lawson Health Research Institute, kstlawr@uwo.ca

Hai Ling Margaret Cheng
Hospital for Sick Children University of Toronto

JOURNAL OF MAGNETIC RESONANCE IMAGING 34:608–615 (2011)

Original Research

Quantification of Renal Perfusion: Comparison of Arterial Spin Labeling and Dynamic Contrast-Enhanced MRI

Jeff D. Winter, PhD,[1] Keith S. St. Lawrence, PhD,[2,3] and Hai-Ling Margaret Cheng, PhD[1,4]*

Purpose: To provide the first comparison of absolute renal perfusion obtained by arterial spin labeling (ASL) and separable compartment modeling of dynamic contrast-enhanced (DCE) magnetic resonance imaging (MRI). Moreover, we provide the first application of the dual bolus approach to quantitative DCE-MRI perfusion measurements in the kidney.

Materials and Methods: Consecutive ASL and DCE-MRI acquisitions were performed on six rabbits on a 1.5 T MRI system. Gadolinium (Gd)-DTPA was administered in two separate injections to decouple measurement of the arterial input function and tissue uptake curves. For DCE perfusion, pixel-wise and mean cortex region-of-interest tissue curves were fit to a separable compartment model.

Results: Absolute renal cortex perfusion estimates obtained by DCE and ASL were in close agreement: 3.28 ± 0.59 mL/g/min (ASL), 2.98 ± 0.60 mL/g/min (DCE), and 3.57 ± 0.96 mL/g/min (pixel-wise DCE). Renal medulla perfusion was 1.53 ± 0.35 mL/g/min (ASL) but was not adequately described by the separable compartment model.

Conclusion: ASL and DCE-MRI provided similar measures of absolute perfusion in the renal cortex, offering both noncontrast and contrast-based alternatives to improve current renal MRI assessment of kidney function.

Key Words: perfusion; arterial spin labeling; dynamic contrast enhanced MRI; kidney; cortex; rabbit
J. Magn. Reson. Imaging 2011;34:608–615.

RENOVASCULAR DISEASE is a major cause of renal hypertension, ischemia, and injury, and may progress to endstage renal failure. Evidence suggests that renovascular disease is linked to damage or loss of renal microvessels, showing that this etiology plays a key role in disease progression and severity (1,2). Current novel treatment strategies target the vasculature by stimulating angiogenesis to offset loss of microvessels, which is thought to arise from impaired capillary repair or impaired endothelial proliferative response (1). Therefore, measuring renal microvascular perfusion is necessary both in the assessment of renovascular diseases and in monitoring therapeutic interventions. However, typical clinical assessment of kidney function does not measure absolute perfusion, as the glomerular filtration rate (GFR), a quantity representing the flow rate of fluid filtered through the kidney, is the primary index. A noninvasive measure of absolute renal perfusion can provide additional information to improve assessment in both diagnosis and evaluation of treatment efficacy.

Two magnetic resonance imaging (MRI) techniques currently exist for renal perfusion measurement: dynamic contrast-enhanced (DCE)-MRI and arterial spin labeling (ASL). Quantitative DCE-MRI involves the injection of a contrast agent, usually gadolinium (Gd)-based, and pharmacokinetic analysis of contrast uptake to extract absolute perfusion. In principle, perfusion can be obtained in addition to the GFR (3–5), but pharmacokinetic models of higher complexity are required in the kidney to distinguish perfusion from filtration-influenced contrast distribution. Various models have been proposed: deconvolution (6,7), 2-compartment separable compartment model (3–5), 3-compartment models (8,9), and a 7-compartment model (10). The potential to reap greater specificity from using higher-order models depends on the available signal-to-noise (SNR) and the ability to obtain a high temporal resolution arterial input function (AIF).

An emerging alternative to quantitative renal perfusion is ASL, which utilizes endogenous blood water as a contrast agent. An advantage of not involving contrast injection is eliminating the risk of nephrogenic systemic fibrosis (NSF) in patients with compromised

[1]Research Institute, Diagnostic Imaging, Hospital for Sick Children, Toronto, Canada.
[2]Imaging Division, Lawson Health Research Institute, London, Canada.
[3]Department of Medical Biophysics, University of Western Ontario, London, Canada.
[4]Department of Medical Biophysics, University of Toronto, Toronto, Canada.
Contract grant sponsor: Natural Sciences and Engineering Research Council of Canada; Contract grant sponsor: Canadian Institutes of Health Research.
*Address reprint requests to: H.-L.M.C., Hospital for Sick Children, 555 University Ave., Toronto, Ontario, Canada M5G 1X8.
E-mail: Hai-Ling.Cheng@sickkids.ca
Received December 7, 2010; Accepted April 29, 2011.
DOI 10.1002/jmri.22660
View this article online at wileyonlinelibrary.com.

kidney function (11). Although principally employed for cerebral blood flow quantification, ASL has begun to see applications outside of the brain, with the kidney being one of the first and most popular sites. Several studies have demonstrated the feasibility of ASL quantification of renal perfusion in both healthy and disease states (12–16). However, a number of quantification issues remain to be addressed, such as: how perfusion estimates may be confounded by different flow characteristics, the positioning and orientation of the tagging slab, and tissue and arterial transit times. Therefore, comparison against an alternate MRI perfusion technique is needed to establish the validity of ASL measurements in the kidney.

Direct comparisons of DCE-MRI and ASL renal perfusion measurements are limited. In this study our objective was to compare renal perfusion estimates obtained from a pulsed ASL technique with those from DCE-MRI calculated using both a pixel-wise and region-of-interest (ROI)-based approach. A separable compartmental model previously demonstrated for pixel-wise DCE mapping of cortical perfusion (5) was employed, and a dual-bolus approach (17) was adopted to provide an accurate, high temporal resolution AIF. This AIF approach, which enables very rapid temporal sampling by introducing a separate low-dose Gd scan, will be applied for the first time in the kidney in this study.

MATERIALS AND METHODS

All procedures were approved by our institutional Animal Care Committee and conducted in accordance with the national standards on animal care. A total of six male New Zealand white rabbits (4.0–4.5 kg) were imaged in this study.

Animal Preparation

Rabbits were induced using a combination of ketamine and xylazine (Akmezine). A catheter was inserted into the ear vein for Gd-DTPA contrast agent injection and for saline infusion (4 mL/kg/h) to maintain fluid levels. During MRI, 100% O_2 was delivered via facemask at 2 L/min in 2% isoflurane for maintenance anesthesia. Heart rate and oxygen saturation were continuously monitored using a pulse oximeter.

MRI

Rabbits were scanned feet first (prone) on a 1.5 T GE scanner (Signa EXCITE TwinSpeed; General Electric Healthcare, Milwaukee, WI). ASL acquisition was performed using an eight-channel receive-only head coil. DCE acquisition was performed using a quadrature transmit/receive knee coil to allow imaging of the aorta for AIF measurement.

ASL

ASL acquisition was performed using a fluid alternating inversion recovery (FAIR) sequence with multislice spiral imaging: echo time (TE) = 4 msec, repetition time (TR) = 3.75 sec, field-of-view (FOV) = 160 mm, matrix = 64 × 64, slice thickness (SL_{TH}) = 5 mm, slice spacing (SL_{SP}) = 1 mm, number of slices (N_{SL} = 3), and postlabel delay time = 1.39 sec. Arterial spatial saturation (30 mm width) was applied 10 mm inferior to the imaging slab at a postlabel delay of 0.7 sec to define the bolus duration. A venous saturation pulse was applied superior to the imaging slab. Background suppression was employed to reduce the influence of motion and physiological noise on the ASL data (18). A total of 64 tag and control image pairs were acquired.

ASL data analysis was performed using custom MatLab (v. 7.0, MathWorks, Natick, MA) and IDL scripts IDL (Interactive Data Language, Research Systems, Boulder, CO). The blood flow (B_F) was calculated from the mean of the ΔM images using the following equation (19):

$$\frac{\Delta M}{M_0} = -\frac{2\alpha}{\lambda} \cdot B_F \cdot e^{-R_{1a} \cdot T_I} \times \left[\frac{(1 - e^{-\Delta R_1 \cdot (T_I - \tau)})}{\Delta R_1} + (\tau + d - T_I) \right] \quad [1]$$

where α (0.85) accounts for signal decrease caused by imperfection in the background-suppression inversion pulses, λ (0.9 mL/g) is the water partition coefficient, R_{1a} (1/1270 $msec^{-1}$) is the longitudinal relaxation rate of arterial water (20), $\Delta R_1 = R_{1a} - R_{1tissue}$, $R_{1tissue}$ is the tissue R_1 that was set to 996 msec for the cortex and 1412 msec for the medulla (21), T_I is the inversion time (adjusted for each slice), τ is the tissue transit time determined in this study, and d is the temporal delay between the tag and arterial saturation.

To determine arterial transit times, a separate acquisition was performed in one rabbit at a series of 11 different postlabel delay times between 0.2 and 3 sec. Sixteen ΔM images were collected for each postlabel delay time. Due to the variable T_I in these experiments, background suppression and arterial spatial saturation pulses were not used. Mean cortex and medulla time series data were fit to the following set of equations (22):

$$\frac{\Delta M(t)}{M_0} = 0, \quad \text{for } 0 \le T_I \le \tau_a$$

$$\frac{\Delta M(t)}{M_0} = -\frac{2\alpha}{\lambda} \cdot B_F \cdot e^{-R_{1a} \cdot T_I} \times \left[\frac{(1 - e^{-\Delta R_1 \cdot (T_I - \tau)})}{\Delta R_1} + (\tau - \tau_a) \right], \quad \text{for } \tau_a \le T_I \le \tau_d$$

$$\frac{\Delta M(t)}{M_0} = -\frac{2\alpha}{\lambda} \cdot B_F \cdot e^{-R_{1a} \cdot \tau_d} \times \left[\frac{(1 - e^{-\Delta R_1 \cdot (\tau_d - \tau)})}{\Delta R_1} + (\tau - \tau_a) \right] \times e^{-R_1 \cdot (T_I - \tau_d)}, \quad \text{for } T_I \ge \tau_d \quad [2]$$

In this set of equations, τ_a represents the arterial transit time and τ_d represents the approximate transit time for the trailing edge of spins flowing into the tissue. After τ_d, labeled arterial proton magnetization remaining in the tissue decays with the tissue R_1 rate.

DCE-MRI

DCE-MRI acquisition was performed immediately following ASL imaging. A dual bolus protocol was used

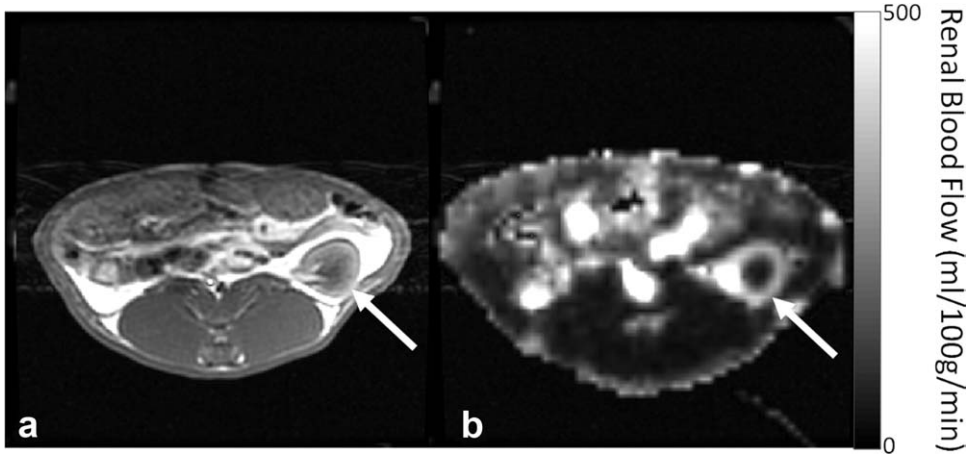

Figure 1. (a) Representative anatomical image and **(b)** corresponding ASL renal blood flow image acquired at the same slice position. Renal blood flow maps were interpolated to 256 × 256 to match the anatomical image resolution. White arrows identify the kidney cortex.

(17): low-dose prebolus injection for AIF measurement followed by a full-dose bolus injection for renal uptake. Gd-DTPA (0.2 mmol kg^{-1}) was split into 20% for the prebolus and 80% for the main bolus, both diluted with saline to maintain a constant injection volume of 0.4 mL kg^{-1}. Contrast was injected with a power injector (Spectris Solaris, Medrad, Warrendale, PA) at a rate of 0.5 mL s^{-1} into the ear vein catheter via a one-way valve, followed by a 2-mL saline "chaser."

Acquisition of the AIF was performed using a 3D TRICKS (time-resolved imaging of contrast kinetics) (23) sequence with one slice running parallel down the aorta. TRICKS is a dynamic fast gradient-recalled echo sequence with an accelerated temporal resolution achieved by sampling low frequency segments of *k*-space at a greater rate than high spatial frequency segments. It was employed in this study to adequately sample the rapid contrast kinetics for the aortic determination of the AIF. Imaging parameters were: TE = 1.02 msec, TR = 2.94 msec, flip angle (FA) = 20, FOV = 180 mm with 70% phase FOV, matrix = 90 × 90, N_{SL} = 10, SL_{TH} = 3 mm, number of averages N_{AVG} = 0.75, and a temporal resolution of 0.554 sec. The AIF was acquired in five separate acquisitions, each containing 56 timepoints and spaced 1 minute apart.

Approximately 15–25 minutes following the prebolus injection, DCE-MRI was performed on the kidney. Quantitative T1 mapping was performed using 3D fast spoiled gradient recalled (FSPGR) echo scans acquired with different FAs (24): TE = 3.1 msec, TR = 7.2 msec, FA = 2, 10, 21°, FOV = 160 mm, matrix = 256 × 192, SL_{TH} = 4 mm, SL_{SP} = 0 mm, N_{SL} = 10, N_{AVG} = 4. A full bolus scan was then performed using 3D FSPGR with the following parameters: TE = 1.86 msec, TR = 4.9 msec, FA = 15°, FOV = 160 mm, matrix = 128 × 96, SL_{TH} = 4 mm, SL_{SP}= 0 mm, N_{SL} = 10, N_{AVG} = 0.75 and temporal resolution = 2.805 sec.

Data were transferred to an independent workstation for analysis. The AIF was determined using a small ROI positioned within the aorta distal to the branch of the renal artery. This location was selected as it was far enough down the aorta to avoid inflow effects, yet in a region of the aorta with a large-enough diameter to minimize partial volume effects. The AIF was extracted from this region by averaging pixels with similar baseline and peak amplitude values. The tail of the AIF was fit to a biexponential decay to provide complete sampling of AIF to reduce noise related to respiratory motion. The AIF signal intensity time curves were converted to Gd concentration ([Gd]) curves to generate $C_a(t)$ using an assumed baseline rabbit blood T_1 of 1270 msec, the FSPGR signal equation, an assumed hematocrit of 0.45, and a linear scale factor relating DCE changes in $\Delta R_1(t)$ with [Gd] (4.1 L/mmol/s).

Kidney tissue uptake curves were then generated. Preinjection T_1 values were calculated from the variable flip angle data and corrected for B_1 variations (24). Mean renal cortex and mean medulla tissue curves were extracted, as well as pixel-wise cortical tissue curves. The tissue curves were converted to [Gd] using baseline T_1 values obtained from the renal T_1 maps using the same procedure as for the AIF. The resulting tissue concentration curve, C(t), was fit to the separable compartmental model (3,5), which considers plasma and the tubular system as separate compartments. Tissue plasma concentration is described by:

$$C_p(t) = \frac{e^{-t/T_p}}{T_p} \otimes C_a(t) \quad [3]$$

where T_p is the plasma transit time and is assumed to be exponentially distributed in the renal plasma. Tubule contrast concentration is represented by:

$$C_T(t) = \frac{F_T e^{-t/T_T}}{V_T} \otimes C_p(t) \quad [4]$$

where F_T is the tubule flow rate, T_T is the tubule transit time, and V_T is the tubular volume that can also be expressed as $V_T = T_T \times F_T(1 - f)$. Together, the separable compartmental model can be expressed as (5):

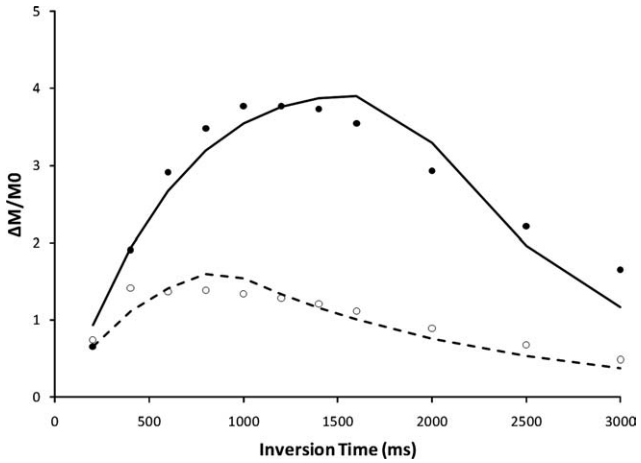

Figure 2. Mean renal cortex (solid circles) and medulla (open circles) signal intensity for the multiple ASL $\Delta M/M_0$ values at each label inversion time. Best fit lines for Eq. [2] in the cortex (solid line) and medulla (dashed line) are shown.

$$C(t) = F_p T_p C_p + F_T e^{-t/T_T} \otimes C_p(t) \quad [5]$$

After visually estimating the delay between *C(t)* and $C_p(t)$, the separable compartment model was fit to *C(t)*. The optimization routine fitted three parameters (F_p, F_T, and T_T) over a range of fixed T_p values between 0 and 30 sec.

Perfusion estimates from ASL and DCE-MRI were compared using a two-tailed Student's *t*-test. In addition, DCE-MRI parameter estimates were compared between the pixel-wise and ROI-based measurements using two-tailed Student's *t*-tests.

RESULTS

All ASL acquisitions were successful on the first attempt, but data were not obtained from one rabbit due to susceptibility artifacts, likely related to excessive gases in the intestinal track. A representative ASL image of renal blood flow is provided in Fig. 1. Despite the low resolution of the ASL image, the renal cortex is clearly distinguishable from the medulla. For the ASL images at varying postlabel delay times, mean cortical and medulla ASL signal ($\Delta M/M_0$) values were fit to Eq. [2], which included an additional term to account for the efflux of labeled spins from the renal parenchyma (Fig. 2). In the cortex, the fitted ASL parameters were: $\tau_a = 0.11$ sec, $\tau = 0.75$ sec, $\tau_d = 1.85$ sec and $B_F = 3.9$ mL/g/min. In the medulla, the best fit curve produced medulla arterial (τ_a) and tissue transit (τ) times that were approximately zero, with $\tau_d = 0.9$ sec and $B_F = 1.74$ mL/g/min.

Representative TRICKS images of the aorta at baseline and peak prebolus contrast for AIF determination are provided in Fig. 3, along with the position of the AIF ROI. Figure 4 shows the main bolus kidney DCE images from the same animal acquired at three different phases: baseline, peak concentration, and 9 minutes postinjection. Regions of the cortex demonstrate a greater initial contrast uptake; however, by the end of the imaging interval, similar signal intensities were observed in the cortex and medulla. The separable compartmental model fit to the mean renal cortex contrast concentration curve is shown in Fig. 5, with the population-based AIF overlaid; note that this model fails to represent tracer kinetics within the renal medulla.

Mean ASL renal perfusion values and DCE-MRI fit parameters are provided in Tables 1 and 2, respectively. ASL perfusion measurements were not available from one rabbit due to considerable susceptibility artifacts, likely due to intestinal gas. Also, only cortical DCE results are shown. Mean renal cortex perfusion estimated by DCE (2.98 ± 0.60 mL/g/min) and ASL (3.28 ± 0.59 mL/g/min) were in close agreement, and no statistical differences were observed between the

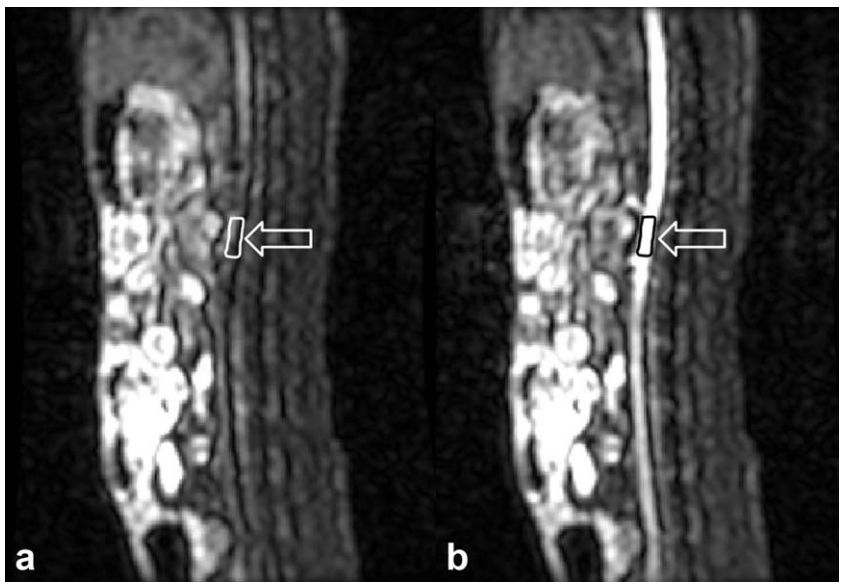

Figure 3. Representative TRICKS images of the aorta at **(a)** baseline and **(b)** peak contrast phases of the DCE-MRI acquisition. The aortic ROIs for AIF extraction are outlined in white in frame A and black in frame B, as indicated with the arrows.

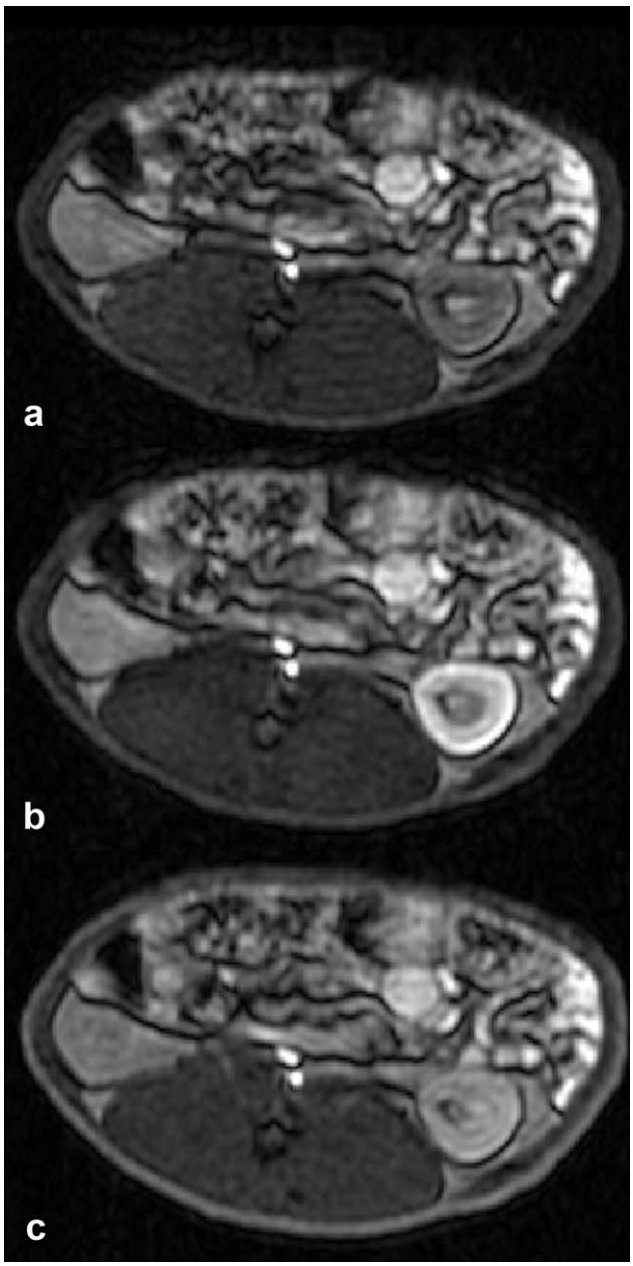

Figure 4. DCE images at **(a)** baseline, **(b)** peak contrast within the renal cortex, and **(c)** ≈9 minutes postinjection. The renal cortex and medulla can easily be distinguished in panel B, which was used in the segmentation of the cortex.

two methods. Signal intensity time curves in the renal cortex provided sufficient SNR to fit the separable compartment model on a pixel-wise basis, as evident from DCE parameter maps shown in Fig. 6. Cortical DCE parameters generated from pixel-wise and mean ROI-based cortical uptake curves provided similar values for most parameters (Table 2); however, F_p was significantly greater for the ROI-based approach ($P < 0.05$).

DISCUSSION

The main result of this study was that ASL and DCE-MRI yielded similar estimates of renal cortex perfusion that are in close agreement with literature reports in the rabbit. In our study, cortex perfusion was 3.28 ± 0.59 mL/g/min (ASL), 2.98 ± 0.60 mL/g/min (DCE), and 3.57 ± 0.96 mL/g/min (pixel-wise DCE); medulla perfusion was 1.53 ± 0.35 mL/g/min (ASL). These numbers are comparable to a mean cortical flow rate of 2.5 ± 1.1 mL/g/min measured in rabbit kidneys using a renal vein outflow method (25). They also fall within the perfusion range reported in a detailed investigation in the rabbit kidney performed using radioactive microspheres, where perfusion rates from 6.1 ± 1.14 to 1.8 ± 0.25 mL/g/min were measured in transversing the outer to inner cortex (26). In an orthotopic transplantation study, a flow rate of 3.7 ± 1.0 mL/g/min was used to perfuse isolated rabbit

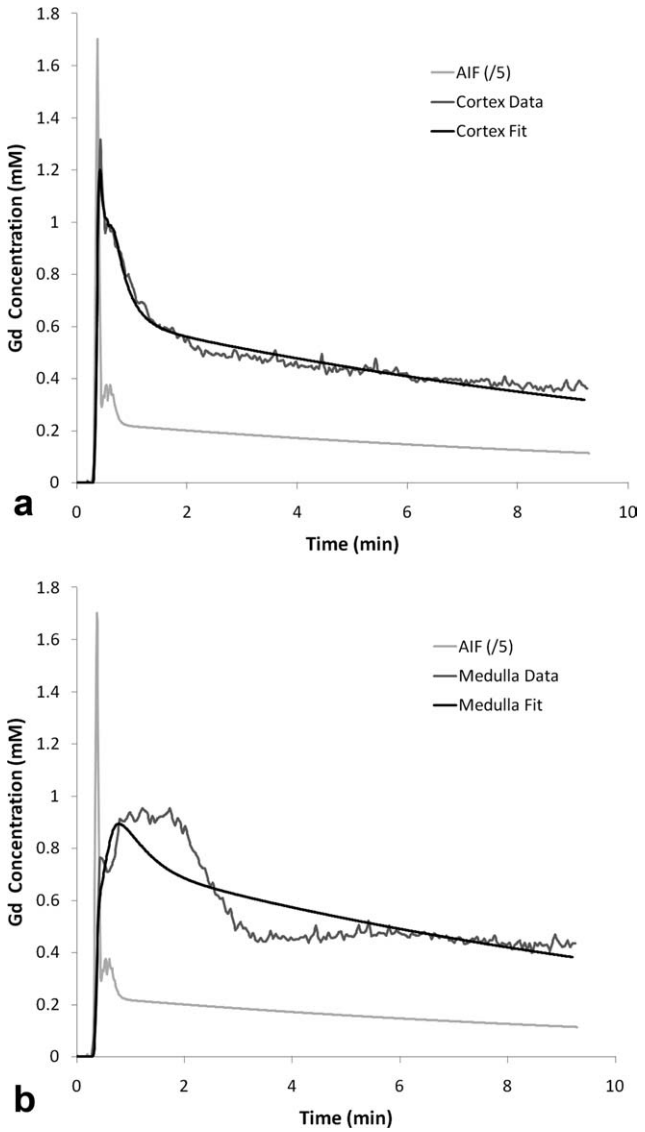

Figure 5. Fit of the separable compartmental model to the mean DCE contrast concentration curves in renal **(a)** cortex and **(b)** medulla in a representative rabbit, after correcting for the delay between the two signals. The population-averaged AIF is also shown, but downscaled by a factor of 5 for visual display purposes. The tail portion of the AIF is the fit to a biexponential function.

Table 1
ASL Estimates of Renal Blood Flow in the Left Kidney

Rabbit	Cortex	Medulla
B	3.09	1.47
C	4.24	1.85
D	2.96	1.82
E	2.70	0.97
F	3.41	1.52
Mean	3.28 ± 0.59	1.53 ± 0.35

Blood flow in units of mL/g/min. ASL measures not available for rabbit A due to considerable susceptibility effects.

kidneys to maintain homeostasis (27). On comparing medullary to cortical perfusion, several studies reported a 3-fold decrease in the medulla, similar to our results, but provided only relative perfusion units (28,29). MRI studies of renal perfusion quantification in rabbits are not available for comparison, but parallels can be drawn to several DCE-MRI and ASL human studies given the similar perfusion rates in rabbits and humans. Most notably, a previous human study using the separable compartmental model reported similar cortical perfusion (3.09 ± 0.45 mL/g/min) (5). ASL measurements in the current study also agree with previous ASL studies that reported cortical perfusion values of 2.78 ± 0.55 mL/g/min (16) and 3.23 ±0.59 mL/g/min (30) using a similar FAIR ASL approach.

Another interesting observation from this study was the significant difference between DCE-MRI measures of perfusion using the pixel-wise and mean ROI-based approach for extracting cortical contrast uptake curves. This difference is likely attributed to the increased DCE-MRI SNR for the tissue uptake curve with the ROI-based method, and the reduced partial volume effects with the pixel-based analysis. It is difficult to suggest the optimal approach. However, in situations where regional differences in cortical perfusion are expected, the pixel-wise approach will clearly be more appropriate than an ROI-based method.

A significant advantage of quantitative DCE-MRI is that functional parameters beyond perfusion can be extracted, including information related to the tubule compartment. In the separable compartment model, tubule compartment parameters (F_T and T_T) can be combined with parenchymal volume and relative cortical volume fraction to estimate GFR. Literature values for rabbit F_T and T_T are not available for comparison. However, the large discrepancy between our values ($F_T = 0.97 \pm 0.29$ mL/g/min, $T_T = 23.3 \pm 8.4$ sec) and those reported in humans ($F_T = 22 \pm 11$ mL/g/min, $T_T = 123 \pm 62$ sec) (5) underscores physiological differences across species, differences in contrast agent (Sourbron et al (5) utilized Gd-BOPTA, a contrast agent that is dependent on albumin concentration), or the recognized challenge of obtaining accurate tubule parameters using DCE-MRI. Lack of accurate tubule parameter estimation via DCE-MRI is also supported by a previous GFR validation study in the rabbit kidney, which showed that DCE-MRI measures of absolute GFR were underestimated compared with reference GFR calculated via ^{51}Cr-ethylenediaminetetraacetic-acid (3).

ASL provides several key advantages over DCE-MRI for the assessment of renal perfusion. First and foremost, ASL uses endogenous blood water as a contrast agent and does not involve the injection of Gd-based contrast agents. Therefore, it may be the only viable option for patients who have impaired renal function, due to the potential risk of developing NSF from delayed clearance of Gd through the kidneys. The lack of contrast injection in ASL also provides an opportunity to conduct longitudinal studies to track disease progression and to monitor the efficacy of novel therapeutic interventions. Another key advantage is that quantification does not require an AIF and the ASL signal is directly related to perfusion. Limitations include coarser spatial resolution (issues with distinguishing the tubule system) and intrinsically low SNR, particularly in cortical regions with reduced perfusion due to pathology and also within the medulla. In translating the ASL technique outside of the brain, organ-specific modifications to the typical general kinetic model were required. In the current protocol, this modification was achieved by determining the arterial and tissue transit times of the renal cortex (through fitting a simple compartmental model to data acquired at different T_I), both of which were shorter than cerebral transit times (31). More recent ASL approaches employ multiple inversion times to directly estimate the transit time on a voxel-by-voxel

Table 2
DCE-MRI Renal Cortex Parameters in the Left Kidney

	F_p (mL/g/min)		T_p (s)		F_T (mL/g/min)		T_T (s)	
Rabbit	Cortical ROI	Pixel-wise	Cortical ROI	Pixel-wise	Cortical ROI	Pixel-wise	Cortical ROI	Pixel-wise
A	2.12	2.48	9.0	10.5	0.50	0.66	39.3	38.8
B	3.03	4.10	3.6	5.4	0.94	1.24	22.3	22.5
C	2.65	2.81	6.0	7.6	0.89	1.07	19.2	17.6
D	2.84	2.89	3.6	5.9	1.37	1.22	15.9	15.4
E	3.82	4.80	3.0	2.2	1.10	1.38	18.3	17.8
F	3.43	4.34	3.0	3.1	1.01	1.22	24.8	23.1
Mean	2.98 ± 0.60*	3.57 ± 0.96	4.7 ± 2.4	5.8 ± 3.0	0.97 ± 0.29	1.1 ± 0.3	23.3 ± 8.4	22.5 ± 8.5

Cortical region-of-interest (ROI) values generated by fitting mean cortical signal to the separable compartment model. Pixel-wise values represent average parameter value obtained by fitting each pixel individually.
*$P < 0.05$ between ROI and pixel-wise parameter estimates.

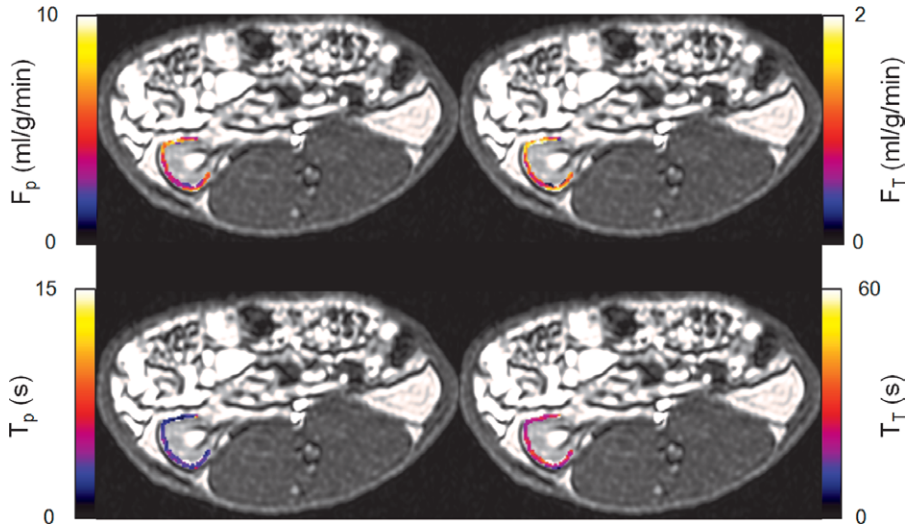

Figure 6. DCE parameter maps of plasma flow (F_p), plasma transit time (T_p), tubule flow (F_T), and tubule transit time (T_T) overlaid on a preinjection baseline DCE image.

basis (32), but this approach does not yet yield the temporal dynamic range needed to extract renal filtration estimates.

Quantification of perfusion in the renal medulla using MRI is challenging. Although our ASL medulla perfusion estimate of 1.53 ± 0.35 mL/g/min agrees with the 3-fold reduction relative to cortical perfusion reported in the rabbit kidney (28,29), estimating medulla perfusion is prone to partial volume effects. This source of error, which is greatest near the boundary of the cortex as well as at the interface of the inner and outer medulla, may account for the reported variation (0.55 ± 0.25 to 2.23 ± 0.76 mL/g/min in humans (16,33)) from ASL approaches. In the current study, partial volume effects were likely responsible for the poor estimation of transit time from the $\Delta M/M_0$ measurements at different T_I. For DCE-MRI, we found that the separable compartment model was inadequate for fitting the contrast kinetics within the kidney medulla. Likewise, previous applications of the separable compartment model did not focus on the medulla but fitted instead the mean whole kidney, mean cortical, and pixel-wise cortical DCE signal changes (5). More complex compartmental models that account for dynamic contrast changes are likely required to provide estimates of global medulla perfusion (9).

The separable compartment model employed in this study is only one of several approaches for estimating renal perfusion. A model-free approach may alternatively be taken, such as deconvolution techniques to extract estimates of both the mean transit time and perfusion, but the deconvolution procedure can be unstable at lower SNR. With compartment model-based approaches, a greater number of compartments may be employed to model kidney dynamics. For example, the Tofts 3-compartment model recently proposed utilizes concentration curves from both the renal cortex and medulla to provide a comprehensive assessment of the complex renal system (8). Additional parameters have also been fitted using a 7-compartment model (10). These models with greater than two compartments generally provide an excellent fit to the DCE-MRI data and better account for the complexities of tracer-kinetics in the kidney. However, unlike the 2-compartment approach adopted in this study, these methods require segmentation of the cortex and medulla and do not permit pixel-wise perfusion estimation.

One unique contribution of this study is the first demonstration of a dual bolus approach (17) to quantitative DCE-MRI within the kidney, a method previously employed in cardiac imaging. A key advantage of this approach is the decoupling of AIF and tissue uptake measurement, which allows the AIF to be sampled with a very high temporal resolution, yet accommodates high spatial resolution when imaging the tissue of interest. Also, the potential for signal saturation is avoided by using a low dose for the AIF prebolus. To account for small residual contrast from the prebolus, T_1 measurements of the kidney were made immediately prior to injection of the main bolus. The accuracy of this technique, specifically, the equivalence of DCE parameters obtained from a dual versus single bolus injection, has been investigated systematically (17).

In conclusion, we demonstrated that renal cortex ASL and DCE estimates of absolute perfusion, averaged across subjects, are in agreement in the normal rabbit kidney. Renal perfusion estimates provide a direct assessment of the renal microvascular status, which is clinically valuable for the assessment of renovascular disease and for monitoring novel angiogenic therapies. These two alternatives are equally capable of measuring renal perfusion and offer a choice to different patient groups. In patients without compromised renal function who can tolerate Gd-injection, DCE-MRI offers the ability to map perfusion at high spatial resolution. In patients where GFR is reduced and, therefore, contraindicated for Gd-injection, ASL provides a potentially valuable alternative for quantifying renal perfusion.

ACKNOWLEDGMENTS

We thank Marvin Estrada, Tammy Rayner, and Ruth Weiss for technical assistance.

REFERENCES

1. Kang DH, Kanellis J, Hugo C, et al. Role of the microvascular endothelium in progressive renal disease. J Am Soc Nephrol 2002; 133:806–816.
2. Iliescu R, Fernandez SR, Kelsen S, Maric C, Chade AR. Role of renal microcirculation in experimental renovascular disease. Nephrol Dial Transplant 2009;25:1079–1087.
3. Annet L, Hermoye L, Peeters F, Jamar F, Dehoux JP, Van Beers BE. Glomerular filtration rate: assessment with dynamic contrast-enhanced MRI and a cortical-compartment model in the rabbit kidney. J Magn Reson Imaging 2004;205:843–849.
4. Buckley DL, Shurrab AE, Cheung CM, Jones AP, Mamtora H, Kalra PA. Measurement of single kidney function using dynamic contrast-enhanced MRI: comparison of two models in human subjects. J Magn Reson Imaging 2006;245:1117–1123.
5. Sourbron SP, Michaely HJ, Reiser MF, Schoenberg SO. MRI-measurement of perfusion and glomerular filtration in the human kidney with a separable compartment model. Invest Radiol 2008; 431:40–48.
6. Hermoye L, Annet L, Lemmerling P, et al. Calculation of the renal perfusion and glomerular filtration rate from the renal impulse response obtained with MRI. Magn Reson Med 2004;515: 1017–1025.
7. Dujardin M, Sourbron S, Luypaert R, Verbeelen D, Stadnik T. Quantification of renal perfusion and function on a voxel-by-voxel basis: a feasibility study. Magn Reson Med 2005;544: 841–849.
8. Cutajar M, Mendichovszky IA, Tofts PS, Gordon I. The importance of AIF ROI selection in DCE-MRI renography: reproducibility and variability of renal perfusion and filtration. Eur J Radiol 2010;74: e154–160.
9. Zhang JL, Rusinek H, Bokacheva L, et al. Functional assessment of the kidney from magnetic resonance and computed tomography renography: impulse retention approach to a multicompartment model. Magn Reson Med 2008;592:278–288.
10. Lee VS, Rusinek H, Bokacheva L, et al. Renal function measurements from MR renography and a simplified multicompartmental model. Am J Physiol Renal Physiol 2007;2925:F1548–1559.
11. Prince MR, Zhang HL, Roditi GH, Leiner T, Kucharczyk W. Risk factors for NSF: a literature review. J Magn Reson Imaging 2009; 306:1298–1308.
12. Boss A, Martirosian P, Schraml C, et al. Morphological, contrast-enhanced and spin labeling perfusion imaging for monitoring of relapse after RF ablation of renal cell carcinomas. Eur Radiol 2006;166:1226–1236.
13. Kiefer C, Schroth G, Gralla J, Diehm N, Baumgartner I, Husmann M. A feasibility study on model-based evaluation of kidney perfusion measured by means of FAIR prepared true-FISP arterial spin labeling (ASL) on a 3-T MR scanner. Acad Radiol 2009;161: 79–87.
14. Schor-Bardach R, Alsop DC, Pedrosa I, et al. Does arterial spin-labeling MR imaging-measured tumor perfusion correlate with renal cell cancer response to antiangiogenic therapy in a mouse model? Radiology 2009;2513:731–742.
15. Warmuth C, Nagel S, Hegemann O, Wlodarczyk W, Ludemann L. Accuracy of blood flow values determined by arterial spin labeling: a validation study in isolated porcine kidneys. J Magn Reson Imaging 2007;262:353–358.
16. Roberts DA, Detre JA, Bolinger L, et al. Renal perfusion in humans: MR imaging with spin tagging of arterial water. Radiology 1995;1961:281–286.
17. Kershaw LE, Cheng HL. A general dual bolus approach for quantitative DCE-MRI. Magn Reson Imaging 2011;29:160–166.
18. St Lawrence KS, Frank JA, Bandettini PA, Ye FQ. Noise reduction in multi-slice arterial spin tagging imaging. Magn Reson Med 2005;533:735–738.
19. Koziak AM, Winter J, Lee TY, Thompson RT, St Lawrence KS. Validation study of a pulsed arterial spin labeling technique by comparison to perfusion computed tomography. Magn Reson Imaging 2008;264:543–553.
20. Ye FQ, Mattay VS, Jezzard P, et al. Correction for vascular artifacts in cerebral blood flow values measured by using arterial spin tagging techniques. Magn Reson Med 1997;372:226–235.
21. de Bazelaire CM, Duhamel GD, Rofsky NM, Alsop DC. MR imaging relaxation times of abdominal and pelvic tissues measured in vivo at 3.0 T: preliminary results. Radiology 2004;2303:652–659.
22. Yang Y, Engelien W, Xu S, Gu H, Silbersweig DA, Stern E. Transit time, trailing time, and cerebral blood flow during brain activation: measurement using multislice, pulsed spin-labeling perfusion imaging. Magn Reson Med 2000;445:680–685.
23. Korosec FR, Frayne R, Grist TM, Mistretta CA. Time-resolved contrast-enhanced 3D MR angiography. Magn Reson Med 1996; 363:345–351.
24. Cheng HL, Wright GA. Rapid high-resolution T(1) mapping by variable flip angles: accurate and precise measurements in the presence of radiofrequency field inhomogeneity. Magn Reson Med 2006;553:566–574.
25. Sadowski J, Kulczykowska E, Kulczykowski M, Badzyñska B. Renal vein outflow recording in rats and rabbits: alternative method of R.B.F. measurement. Acta Physiol Hung 1988;72:335–342.
26. Aizawa C, Honda N. Failure to abolish reactive hyperemia by indomethacin in denervated kidneys of rabbits. Am J Physiol 1977; 233:F89–93.
27. Arnaud FG, Khirabadi BS, Fahy FM. Normothermic blood perfusion of isolated rabbit kidneys. II. In vitro evaluation of renal function followed by orthotopic transplantation. ASAIO J 2000; 46:707–718.
28. Evans RG, Madden AC, Denton KM. Diversity of responses of renal cortical and medullary blood flow to vasoconstrictors in conscious rabbits. Acta Physiol Scand 2000;169:297–308.
29. Patel TY, Hovsepian DM, Duncan JR. Measurement of blood flow before and after embolization with use of fluorescent microspheres in an animal model. J Vasc Interv Radiol 2006;17: 103–111.
30. Fenchel M, Martirosian P, Langanke J, et al. Perfusion MR imaging with FAIR true FISP spin labeling in patients with and without renal artery stenosis: initial experience. Radiology 2006; 2383:1013–1021.
31. Koziak AM, Winter J, Lee TY, Thompson RT, St Lawrence KS. Validation study of a pulsed arterial spin labeling technique by comparison to perfusion computed tomography. Magn Reson Imaging 2008;264:543–553.
32. Hoad CL, Cox EF, Gardner AG, Anblagan D, Francis ST. Multiphase true-FISP ASL in the kidney. In: Proc 18th Annual Meeting ISMRM, Stockholm; 2010 (abstract 327).
33. Robson PM, Madhuranthakam AJ, Dai W, Pedrosa I, Rofsky NM, Alsop DC. Strategies for reducing respiratory motion artifacts in renal perfusion imaging with arterial spin labeling. Magn Reson Med 2009;616:1374–1387.